Detecting non-germinomatous germ cell tumor component by arterial spin labeling perfusion-weighted MR imaging in central nervous system germ cell tumor

Motoki Takano [a], Yasuyuki Kinoshita [a], Kazuhiko Sugiyama [b], Manish Kolakshyapati [a,e], Takeshi Takayasu [a], Ushio Yonezawa [a], Akira Taguchi [a], Yuji Akiyama [c], Vishwa Jeet Amatya [d], Yukio Takeshima [d], Kaoru Kurisu [f], Fumiyuki Yamasaki [a,*]

a *Department of Neurosurgery, Graduate School of Biomedical and Health Sciences, Hiroshima University, 1-2-3 Kasumi, Minami-ku, Hiroshima 734-8551, Japan*
b *Department of Clinical Oncology & Neuro-oncology Program, Hiroshima University Hospital, Hiroshima 734-8551, Japan*
c *Department of Clinical Radiology, Hiroshima University, Hiroshima 734-8551, Japan*
d *Department of Pathology, Graduate School of Biomedical and Health Sciences, Hiroshima University, Hiroshima 734-8551, Japan*
e *Department of Neurosurgery, B & B Hospital, Gwarko, Lalitpur, Nepal*
f *Director, Chugoku Rosai Hospital, 1-5-1 Hirotagaya, Kure, Hiroshima 737-0193, Japan*

ARTICLE INFO

Keywords:
Germinoma
Non-germinomatous germ cell tumor
Relative tumor blood flow
Arterial spin labeling
Apparent diffusion coefficient

ABSTRACT

Purpose: Differentiating between germinoma and non-germinomatous germ cell tumor (NGGCT) is important because sensitivity to chemotherapy and/or radiotherapy is quite different between these two subgroups. In this study, we evaluated whether the arterial spin labeling (ASL) based perfusion-weighted imaging (PWI) could provide additional information for the differential diagnosis between germinoma and NGGCT.
Method: Between 2011 and 2018, 20 patients with central nervous system (CNS) germ cell tumor (GCT) who underwent preoperative MR imaging including ASL-PWI were enrolled in this study. Relative tumor blood flow (rTBF) was evaluated on ASL-PWI by manually placing regions of interest at gadolinium enhanced part of the tumors and normal subcortical white matter. Presence of intratumoral T1 hyperintense foci and apparent diffusion coefficient (ADC) were also evaluated. The final diagnosis was made by the combination of tumor markers and the histological diagnosis.
Results: Among 20 patients of CNS-GCT, 11 were diagnosed as germinoma and 9 were diagnosed as NGGCT. In the germinoma subgroup, the rTBF ranged from 0.90 to 1.71 (mean 1.21, median 1.09), while it ranged from 1.14 to 5.75 (mean 3.91, median 3.31) in NGGCT subgroup. The receiver operating characteristic (ROC) curve showed that calculating rTBF is useful for differentiating between germinoma and NGGCT (area under the curve (AUC) 0.929, P = 0.0012) compared to intratumoral T1 hyperintense foci (AUC 0.788, P = 0.0304) and ADC (AUC 0.919, P = 0.0016).
Conclusions: High rTBF obtained by ASL-PWI implied the presence of NGGCT component. This information might help in deciding the chemotherapy/radiotherapy intensity.

1. Introduction

Central nervous system (CNS) germ cell tumors (GCTs) account for 2–3 % of all primary CNS neoplasms and 8–15 % of pediatric CNS tumors in series from Japan, Taiwan, China and Republic of Korea [1–4]. CNS-GCT develops most often in children aged 10–14 years, with a clear majority in males [1,2,5]. The CNS-GCTs are sub-classified into germinoma and non-germinomatous germ cell tumors (NGGCT). NGGCT consists of teratoma, yolk sac tumor, choriocarcinoma, embryonal carcinoma and mixed tumor of CNS-GCT components, including germinoma component. As the prognosis and sensitivity to treatment are much different between germinoma and NGGCT, physicians need to choose the appropriate treatment considering these two subtypes of GCTs [6]. Previous reports tried to differentiate germinoma and NGGCT by using different MR parameters including T1 hyperintense foci, intratumoral cystic components, tumor margin shape, enhancing pattern, and apparent diffusion coefficient (ADC) calculation and were moderately useful for the differential diagnosis [7–9]. However, differentiation between germinoma and NGGCT is still sometimes difficult because imaging characteristics are not always specific, and biopsy specimens obtained by neuroendoscopic or stereotactic biopsy may not represent the entire tumor and are susceptible to diagnostic errors for mixed GCTs [10]. Arterial spin labeling (ASL) MR imaging is perfusion-weighted imaging (PWI) which uses magnetically labeled arterial blood water protons as an endogenous tracer to allow visualization of perfusion. ASL-PWI can evaluate arterial blood flow without requiring intravenous gadolinium, in other word, non-invasively, therefore, the clinical advantage of ASL-PWI is obviously high compared to other PWI techniques. It has been reported that the ASL-PWI was applied for evaluating acute and chronic neurovascular diseases [11–13], differentiating hemangioblastoma from metastatic brain tumors [14] and determining the degree of the malignancy [15]. However, there has been no report evaluating the histological subtype of GCT using ASL-PWI or other PWI techniques for the differential diagnosis of germinoma and NGGCT. In this study, we showed the utility of ASL-PWI for detecting NGGCT component.

2. Materials and methods

2.1. Patients

The institutional review board approved this retrospective study (IRB No. 2961/E-1601). Between 2011 and 2018, 25 patients with GCT were treated in our institute. Among them, 5 were excluded because of lack of ASL-PWI imaging (4 patients) and too small size of tumor (1 patient). Finally, 20 patients with GCT were included in this study. The final diagnosis of the GCT components was based on the following findings: 1) surgical specimen obtained by biopsy and/or salvage surgery, 2) serum levels of alpha-fetoprotein (AFP) and beta-human chronic gonadotropin (β-HCG). We used the cut-off value of serum AFP ≥ 25ng/mL and/or serum β-HCG ≥ 50IU/L for the diagnosis of NGGCT according to SIOP CNS GCT 96 [16]. The tumor specimens were diagnosed by the consensus of 2 authors (V.J.A. and Y.T.). The mixed GCT with mature/immature teratoma components was classified as NGGCT.

2.2. MRI protocols

In this study, Signa Excite HD 3.0tesla (GE Medical Systems, Milwaukee,WI, U.S.A.) was used before December 2016, and Philips IngeniaCX 3.0T (Royal Philips, Amstelplein, Amsterdam, The Netherlands) was used after 2017. All patients underwent pretreatment MR imaging including T1-weighted imaging, T2-weighted imaging, fluid-attenuated inversion recovery (FLAIR) imaging, T2*-weighted imaging, diffusion weighted imaging (DWI), three-dimensional (3D) pseudo-continuous ASL (pCASL)-PWI and post gadolinium contrast transverse, sagittal, coronal T1-weighted imaging. The conventional MRI protocol for Signa Excite HD 3.0tesla were as follows: T1-weighted imaging (repetition time [TR], 450msec; echo time [TE], 18msec; field of view [FOV], 22 × 22cm; matrix size, 288 × 192/1 number of excitations [NEX]; section thickness, 6mm; intersection gap, 1.0mm; and 2 acquisitions), T2-weighed weighted imaging (TR, 4800msec; TE, 100msec; echo train length,: 18, FOV, 22 × 22cm; matrix size: 512 × 320/2 NEX; section thickness, 6mm; intersection gap, 1.0mm; and 1 acquisition), FLAIR imaging (TR, 10,000msec; TE, 140msec; inversion recovery time, 2400msec; FOV, 22 × 22cm; matrix size, 288 × 160/1 NEX; section thickness, 6mm; intersection gap, 1.0mm; and 2 acquisitions), T2*-weighted imaging (TR, 600msec; TE, 12msec; FOV, 22 × 22cm; matrix size, 320 × 192/1 NEX; section thickness, 6mm; intersection gap, 1.0mm; and 1 acquisition). The conventional MRI protocol for Philips Ingenia CX3.0tesla were as follows: T1-weighted imaging (TR,500 msec; TE, 10msec; FOV, 22 × 22cm; matrix size, 288 × 216/1 NEX; section thickness, 5mm; intersection gap, 1.0mm; and 2 acquisitions), T2-weighted imaging (TR, 3000msec; TE, 100msec; echo train length,:15, FOV, 22 × 22cm; matrix size: 512 × 384/2 NEX; section thickness, 5mm; intersection gap, 1.0mm; and 2 acquisition), FLAIR imaging (TR,10,000msec; TE, 130.0msec; inversion recovery time, 2600.0msec; FOV, 22 × 22cm; matrix size, 288 × 230/1 NEX; section thickness, 5mm; intersection gap, 1.0mm; and 3 acquisitions), T2*- weighted imaging (TR, 600msec; TE, 16msec; FOV, 22 × 22cm; matrix size, 320 × 208/1 NEX; section thickness, 5mm; intersection gap, 1.0mm; and 1 acquisition).

2.3. DWI protocol

For DWI at b-1000s/mm2 by Signa Excite HD 3.0tesla, the effective gradient registered 40mT/m and the slew rate was 150mT/m/msec, TR 5000msec, TE 73.2msec, NEX 1, FOV 22cm × 22cm, slice thickness 6mm; intersection gap 1.0mm, number of slices 20, data acquisition matrix 128 × 128, 2 acquisitions. ADC maps were obtained by calculating the signal intensity on DWI at two different b-values (0 and 1000s/mm^2) with the analysis software (Functool, GE Medical Systems). For DWI at b-1000s/mm^2 by Philips Ingenia CX 3.0T, the effective gradient registered 45mT/m and the slew rate was 200 mT/m/msec, TR 5000msec, TE 84msec, NEX 1, FOV 22cm × 22cm, slice thickness 5mm; intersection gap 1.0mm, number of slices 24, data acquisition matrix 96 × 144, 1 acquisition. ADC maps were automatically generated by MR scanner in Philips Ingenia.

2.4. ASL protocol

3D-ASL perfusion imaging by Signa Excite HD 3.0tesla

covered the whole brain using a 3D background suppressed fast-spin-echo stack-of-spiral readout module with 8 in-plane spiral interleaves (TR/TE = 4463/10.2msec, labeling duration = 1500msec, post-labeling delay = 1525msec, no flow-crushing gradients, in-plane matrix = 128 × 128, flip angle = 155°, NEX = 4, slice thickness = 4mm, FOV = 240mm, voxel size = 1.8 × 1.8 × 4mm), and an echo train length of 1 to obtain 30 consecutive axial slices. A 10-mm-thick labeling plane was placed 20mm inferior to the lower edge of the cerebellum. The total scan time was 335s. For each of the 30 volumes unlabeled were subtracted from labeled images and M0 map correction was performed using vendor-supplied software. 3D-ASL perfusion imaging imaged by Philips Ingenia CX 3.0T covered the whole brain using a 3D pCASL acquisition with Gradient and Spin Echo read-out, providing normalized images, using a 4 pulse background suppression scheme (TR/TE = 4188/10msec, labeling duration = 1800msec, post-labeling delay = 2000msec, in-plane matrix = 64 × 64, reconstruction matrix = 80 × 80, flip angle = 90°, NEX = 5, slice thickness = 6mm, FOV = 240mm, voxel size = 3.75 × 5.30 × 6mm, reconstruction voxel size = 3.0 × 3.0 × 6mm, sensitivity encoding phase reduction factor = 1. 5). A 110mm thick label distance determines the distance between the center of imaging stack and the center of the labeling slab. Post labeling delay = 2000msec. The total scan time was 193s. Subtracted imaging series were automatically calculated and ASL normalized images were available. It could be viewed in color or black and white and the numeric results could be obtained by drawing a ROI on the normalized images.

2.5. Imaging processing and analysis

Imaging processing and analyses were performed by consensus of two authors (M.T. & F.Y.). T1 hyperintense foci were visually defined as a spot or region inside the tumor that showed a clearly stronger hyper-intense signal than the normal appearing white matter on T1-weighted image. To determine the ADC value, ROIs (10 – 30mm^2) were manually placed in gadolinium enhanced-tumor regions on ADC maps. The number of ROIs placed depended on the size of the observable part of the enhanced lesion. The ADC values of each tumor, based on 3–8 ROIs on the ADC map were calculated and minimum absolute

values calculated by ADC (ADCMIN) were obtained. On ASL-PWI, signal intensity of each tumor was visually graded as high-intense, iso-intense, or low-intense, by comparing with that of the normal appearing white matter in the same slice. If tumor contained both high- and low-intense components, it was classified as high-intense. The tumor blood flow (TBF) was calculated by manually placing ROIs at the gadolinium enhanced part of the tumor on ASL-PWI. The ROIs (30 - 40mm^2) were placed on at least 3 portions and the maximum TBF (mTBF) value was obtained from the ROIs. The maximum cerebral blood flow (mCBF) was also obtained by putting at least 3 ROIs on the normal appearing subcortical temporal white matter. The relative TBF (rTBF) was calculated by the following formula: rTBF = mTBF/mCBF as described previously [17].

2.6. Statistical analysis

Statistical analyses were performed with GraphPad Prism version 7.00 for Mac (GraphPad Software, La Jolla, California, USA) and SPSS ver. 27.0 (IBM SPSS Inc., Armonk, New York, USA). Fisher's exact test was performed to assess the differences in intratumoral T1 hyperintense foci between germinoma and NGGCT. The distribution of ADCMIN and rTBF in germinoma and NGGCT were compared by Mann-Whitney U test. Preoperative differential diagnosis between germinoma and NGGCT was evaluated by Receiver Operating Characteristic (ROC) curve. Statistical significance was assigned when P < 0.05.

3. Results

3.1. Patient characteristic

Patients' data are summarized in Table 1. Among 20 patients, 11 were diagnosed as germinoma and 9 were diagnosed as NGGCT. Eleven germinoma patients ranging in age from 9 to 29-years (11 male and 0 female, mean 18.4 years, median 19.0 years) were diagnosed based on the pathological findings of the initial biopsy and lower level of AFP and β-HCG. Nine NGGCT patients ranged in age from 4 to 51-years (9 male and 0 female, mean 15.7 years, median 12.0 years). Three of 9 NGGCT

patients were initially diagnosed as germinoma based on the initial biopsy specimen and low serum tumor maker level, and subsequently diagnosed as NGGCT by detection of teratoma component from salvage surgery. Other 6 patients were diagnosed as NGGCT by the high serum level of AFP/β-HCG. Seven of the 9 NGGCT patients were confirmed to have mature or immature teratoma components. Overall, NGGCT contained 1 pure choriocarcinoma, 1 pure immature teratoma and 7 mixed germ cell tumors.

3.2. Neuroimaging

On conventional MR imaging, 6 of 9 NGGCT patients presented with intratumoral T1 hyperintense foci inside the tumor, whereas only 1 germinoma patient presented with intratumoral T1 hyperintense foci (Figs. 1–4). The presence of intratumoral T1 hyperintense foci was significantly more common in the NGGCT group than in the germinoma group (66.7% vs 9.1%, P = 0.017, Fisher's exact test). The ADCMIN values of the germinoma ranged from 0.535 to 0.83, (mean 0.657, median 0.587) and the ADCMIN values of the NGGCT ranged from 0.614 to 1.349 (mean 0.946, median 1.070). The ADCMIN values of solid tumor portions were significantly higher in NGGCT group than in germinoma group (P = 0.001; Mann-Whitney U test). The tumors were also evaluated by ASL-PWI. In germinoma, visually evaluated intensity was low or iso-intense, and no germinoma showed high-intense on ASL-PWI (Fig. 1). On the other hand, 7 of 9 NGGCT showed high-intensity part on ASL-PWI (Figs. 2,3). One pure immature teratoma and 1 mixed GCT with germinoma and immature teratoma (Fig. 4) showed iso-intense on ASL-PWI. The rTBF of the germinoma ranged from 0.90 to 1.71, (mean 1.21, median 1.09) and the rTBF of the NGGCT ranged from 1.14 to 5.75 (mean 3.91, median 3.31). The rTBF of the NGGCT was significantly higher than that of the germinoma (P = 0.0001; Mann-Whitney U test). The ROC curve analysis (Fig. 5, Table 2) showed that the presence of intratumoral T1 hyperintense foci was useful for differentiating between germinoma and NGGCT (area under curve (AUC) 0.788, P = 0.0304). Calculating ADCMIN value was more useful for differentiation between germinoma and NGGCT (AUC 0.919, P = 0.0016). In our results, calculating rTBF is the most

useful for differentiating between germinoma and NGGCT (AUC 0.929, P = 0.0012). The cut off value of $0.82 \times 10^{-3} \text{mm}^2/\text{s}$ for ADCMIN could differentiate germinoma form NGGCT with the best combination of sensitivity (77.8%) and specificity (90.9%), with a positive-predictive value (PPV) of 87.5%, and a negative-predictive value (NPV) of 83.3%, and the cut off value of rTBF 2.1 could more accurately indicated NGGCT (sensitivity 77.8%, specificity 100%, PPV 100%, NPV 84.6%).

4. Discussion

This is the first report that showed the radiological feature of CNS-GCT by ASL-PWI. Our study clearly demonstrated that the rTBF calculation will help in detecting the presence of NGGCT component in histologically diagnosed germ cell tumors, even in cases where the histology of the initial biopsied tissue may mislead showing only germinoma component. Accurate diagnosis and appropriate treatment are essential to avoid under- or over-treatment for GCT patients. Under-treatment may result in increase of recurrence rate, while over-treatment will result in increase of late effect including secondary cancers. Usually, histopathological diagnosis of surgical specimen is most reliable for almost all brain tumors. However, GCT could consist of heterogeneous pathology, and biopsy specimen might not represent the entire tumor. Kinoshita et al. pointed out that the biopsy specimen of the tumor could result in the inadequate/inaccurate diagnosis of the GCTs [10]. Therefore, it is mandatory to develop the diagnostic tool for the accurate diagnosis of GCTs. Aihara et al. [18] reported the usefulness of measuring placental alkaline phosphatase (PLAP) levels in the cerebrospinal fluid. From their report, PLAP of cerebrospinal fluid was upregulated in all intracranial germinoma, while it was not upregulated in all patients without germinoma component. This information might help in excluding the non-germinoma patients, however, germinoma could exist with other GCT components necessitating other reliable biomarker to confirm the differentiation between "pure" germinoma and NGGCT. Development of imaging biomarker may facilitate for differential diagnosis of GCTs. Bithalamic extension of the tumor at pineal lesion may be one of the characteristics of germinoma [19]. However, the sensitivity and specificity are not so high.

Table1. Summary of patient with germinoma and NGGCT

Patient	Final diagnosis	Age	Sex	Tumor location	Method of initial operation	Histological diagnosis at initial surgery	Diagnosis before CTx/RTx	Histological diagnosis at salvage surgery	Serum β-HCG	Serum AFP	T1 hyper-intensity foci	ADCMIN *	Signal intensity of ASL	rTBF
1	germinoma	29	M	P	endoscopic	germinoma	germinoma	N/A	23.4	<5.0	-	0.565	iso	1.02
2	germinoma	19	M	P	endoscopic	germinoma	germinoma	N/A	2.6	<5.0	-	0.935	iso	1.26
3	germinoma	9	M	P	endoscopic	germinoma	germinoma	N/A	18.2	<5.0	+	0.732	iso	1.31
4	germinoma	20	M	P/N	trans sphenoidal	germinoma	germinoma	N/A	40.7	3.3	-	0.582	iso	1.27
5	germinoma	14	M	P	endoscopic	germinoma	germinoma	N/A	<0.1	1.6	-	0.571	iso	1.09
6	germinoma	23	M	P	endoscopic	germinoma	germinoma	N/A	<0.1	0.7	-	0.65	iso	1.07
7	germinoma	20	M	P	endoscopic	germinoma	germinoma	N/A	5.1	1.6	-	0.555	iso	1.08
8	germinoma	10	M	P	endoscopic	germinoma	germinoma	N/A	<0.1	1.3	-	0.810	iso	1.09
9	germinoma	16	M	P	endoscopic	germinoma	germinoma	N/A	<0.1	1.9	-	0.810	low	0.90
10	germinoma	18	M	N	trans sphenoidal	germinoma	germinoma	N/A	<0.1	2	-	0.587	iso	1.47
11	germinoma	24	M	P/N	trans sphenoidal	germinoma	germinoma	N/A	0.3	3.8	-	0.830	iso	1.71
12	NGGCT	19	M	P	endoscopic	N/A	choriocarcinoma	N/A	5410	2.2	+	0.942	high	2.51
13	NGGCT	4	M	P	craniotomy	IT	IT	N/A	<0.1	16.4	+	1.18	iso	1.38
14	NGGCT	51	M	P	endoscopic	yolk sac tumor	mixed GCT	MT	0.2	820.5	-	0.759	high	2.70
15	NGGCT	13	M	P	endoscopic	germinoma	germinoma	IT	0.5	33.2	+	0.614	iso	1.14
16	NGGCT	8	M	P	endoscopic	germinoma	mixed GCT	MT	<0.1	452.7	-	1.349	high	5.75
17	NGGCT	12	M	P/BG	stereotactic	germinoma	germinoma	MT	<0.1	3.3	+	1.343	high	3.91
18	NGGCT	8	M	P	only ETV	N/A	mixed GCT	IT	<0.1	1679.7	+	1.07	high	4.71
19	NGGCT	14	M	P	only ETV	N/A	mixed GCT	MT	<0.1	3111.9	+	1.00	high	4.86
20	NGGCT	12	M	P	endoscopic	germinoma	mixed GCT	MT	<0.1	536.9	-	1.33	high	4.38

NGGCT, non-germinomatous germ cell tumor; M, male; F, female; P, pineal; N, neurohypophyseal; BG, basal ganglia; ETV, Endoscopic third ventriculostomy; MT, mature teratoma; IT, immature teratoma; GCT, germ cell tumor; CTx, chemotherapy; RTx, radiotherapy; ASL, arterial spin labeling; rTBF, relative tumor blood flow; N/A, not applicable; HCG, human chorionic gonadotropin (ng/ml); AFP, α-fetoprotein (mIU/ml); * ADCMIN, minimum absolute value of apparent diffusion co-efficient ($\times 10^{-3}$ mm^2/s)
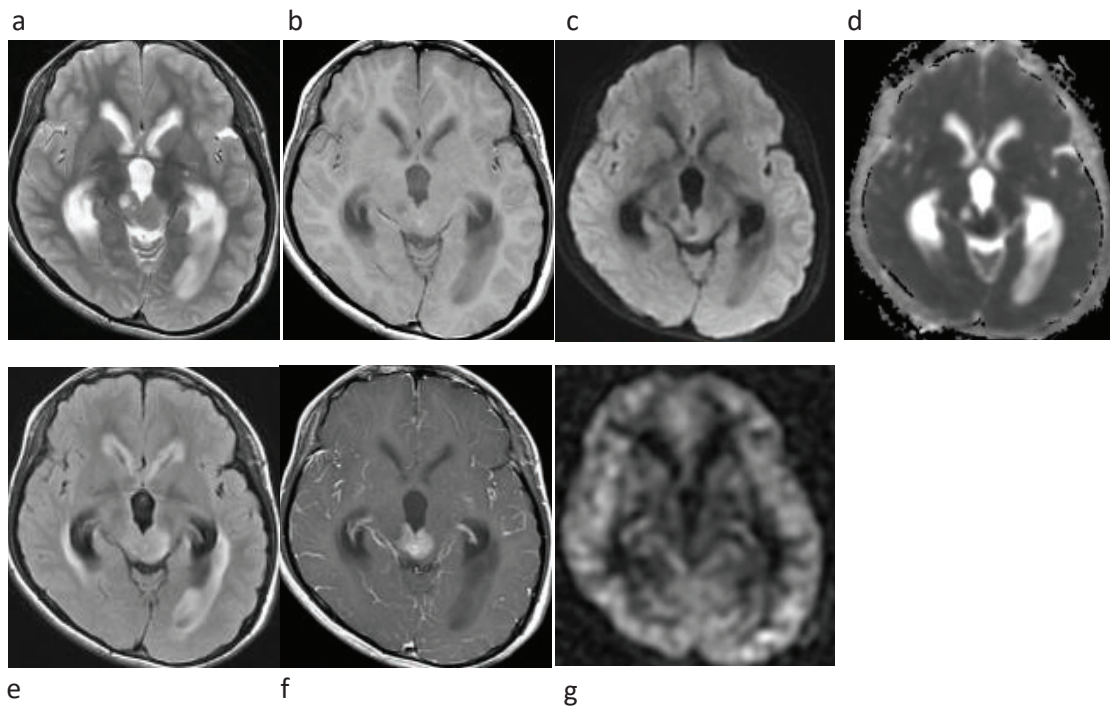
Fig. 1. Germinoma developed at pineal region in a 14-years-old boy (patient 5). The tumor shows iso-intensity on T2-weighted imaging (a) and T1-weighted imaging (b), high-intensity on diffusion-weighted imaging (c) and fluid attenuated inversion recovery imaging (e), and low-intensity on ADC map (d). The tumor is homogeneously enhanced by gadolinium on T1-weighted imaging (f). The arterial spin labeling imaging revealed the low blood flow within the tumor (g).
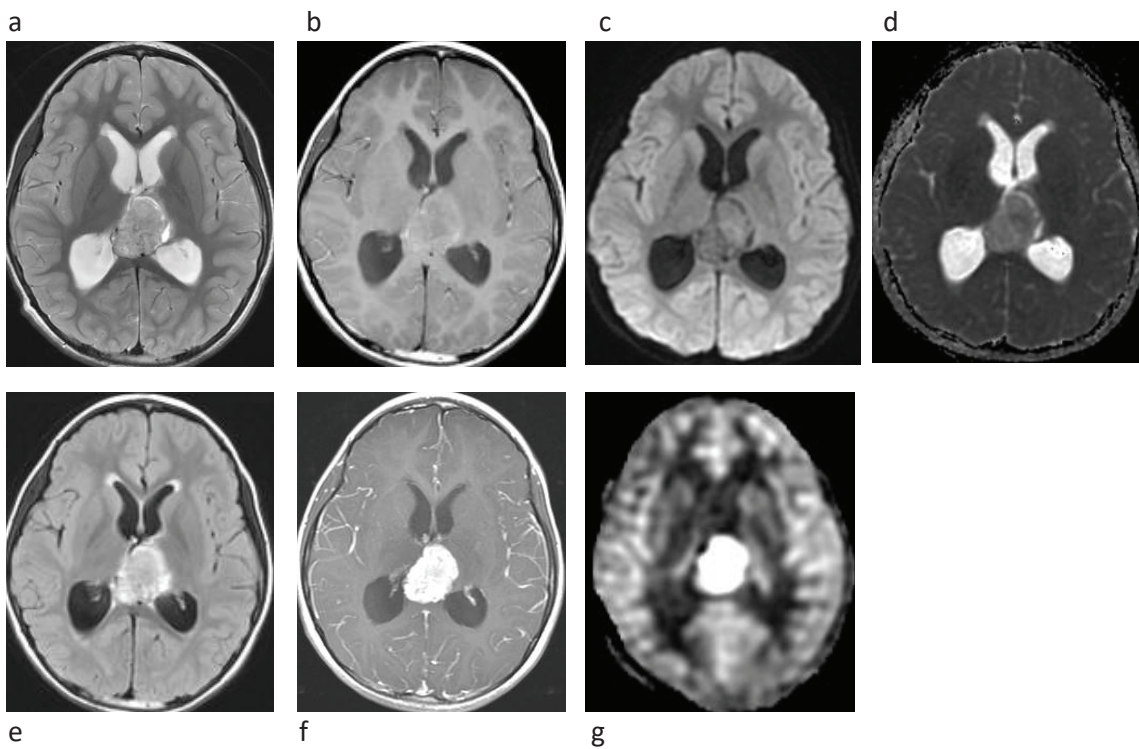
Fig. 2. Mixed germ cell tumor consisting of yolk sac tumor and mature teratoma developed at pineal region in an 8-years-old boy (patient 16). The tumor shows iso-intensity on T2-weighted imaging (a), T1-weighted imaging (b) and diffusion weighted imaging (c), and high-intensity on ADC map (d) and fluid attenuated inversion recovery imaging (e). The tumor is homogeneously enhanced by gadolinium on T1-weighted imaging (f). The arterial spin labeling imaging revealed the high blood flow within the tumor (g).
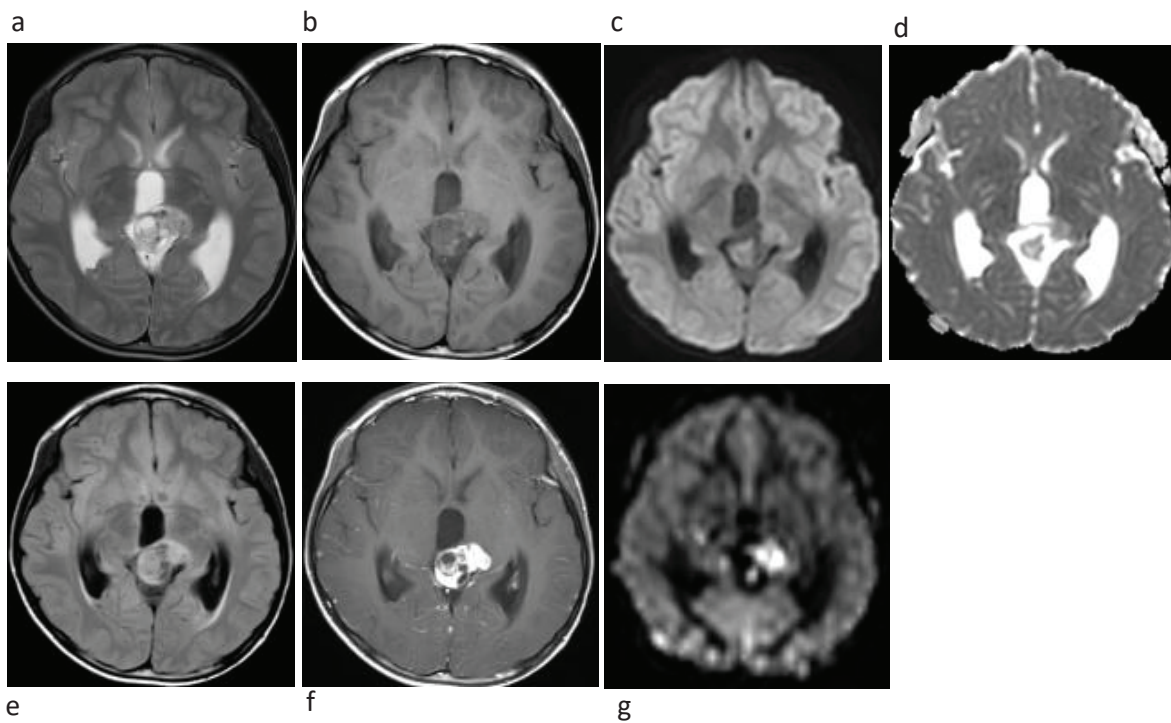
Fig. 3. Mixed germ cell tumor consisting of yolk sac tumor, mature and immature teratoma developed at pineal region in an 8-years-old boy (patient 18). The solid component of the tumor shows iso-intensity on T2-weighted imaging (a), T1-weighted imaging (b) and diffusion weighted imaging (c), and high-intensity on ADC map (d) and fluid attenuated inversion recovery imaging (e). The tumor is heterogeneously enhanced by gadolinium on T1-weighted imaging (f). The arterial spin labeling imaging revealed the tumor had high blood flow and low blood flow components (g).
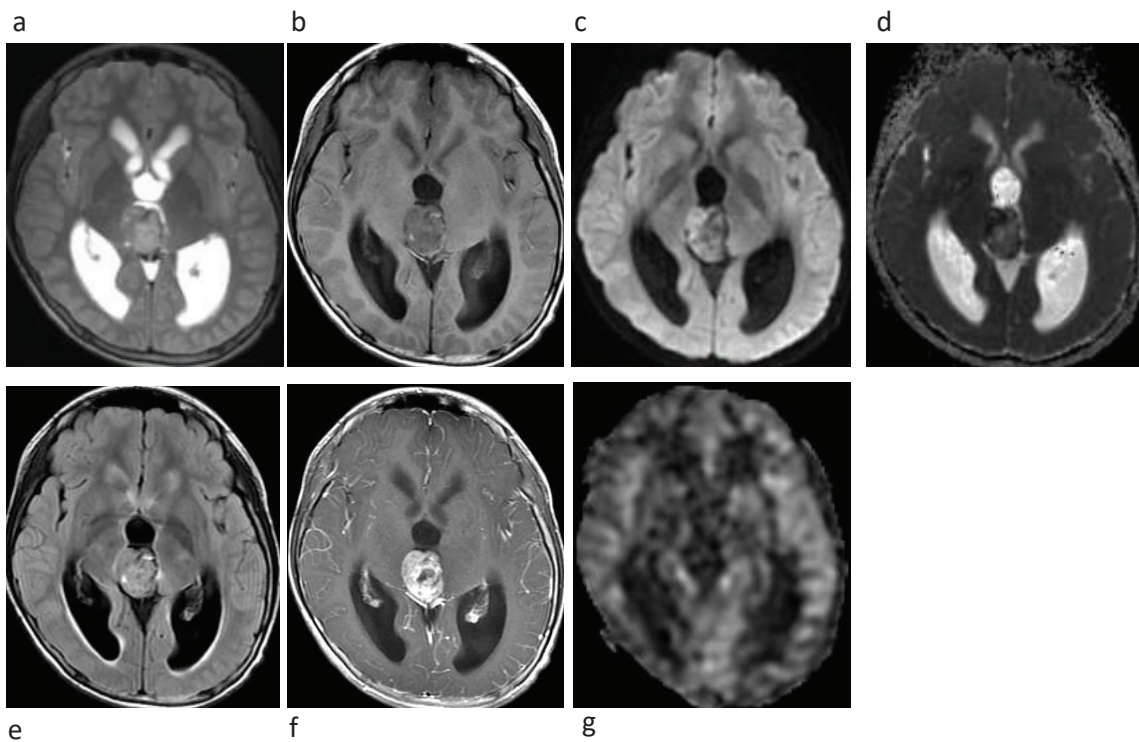
Fig. 4. Mixed germ cell tumor consisting of germinoma and immature teratoma developed at pineal region in a 13-years-old boy (patient 15). The tumor shows high-intensity on T2-weighted imaging (a), iso- to high-intense on ADC map (d), and fluid attenuated inversion recovery (e), and partly high-intensity on diffusion-weighted imaging (c), and low-intensity on T1-weighted imaging (b). The tumor is heterogeneously enhanced by gadolinium on T1-weighted imaging (f). The arterial spin labeling imaging (f) revealed the low blood flow within the tumor.

a) ROC curve of T1 hyperintense foci   b) ROC curve of ADCMIN   c) ROC curve of rTBF
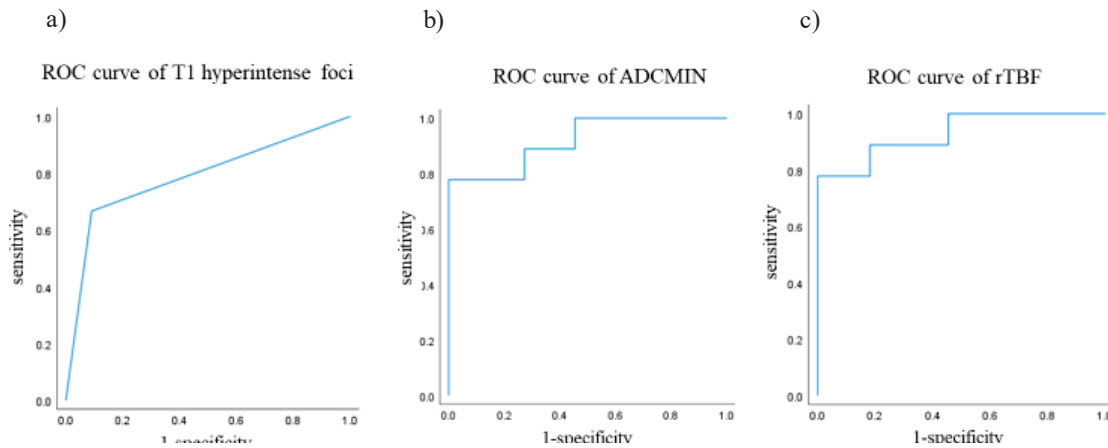
Fig. 5. The ROC curve of the intratumoral T1 hyperintense foci (a), ADCMIN (b) and rTBF (c) demonstrate that the AUC was 0.788 (P = 0.0304), 0.919 (P = 0.0016) and 0.929 (P = 0.0012) respectively. Calculating rTBF is the most useful imaging tool for differentiating between germinoma and NGGCT.

Table 2. Sensitivity, specificity, PPV, and NPV for intratumoral T1 hyperintense foci, ADCMIN and rTBF in the differential diagnosis of NGGCT from germinoma

	Sensitivity (%)	Specificity (%)	PPV (%)	NPV (%)	AUC	P
intratumoral T1 hyperintense foci	66.7	90.9	85.7	76.9	0.788	0.0304*
ADCMIN > 0.82 ×10^{-3} mm^2/s	77.8	90.9	87.5	83.3	0.919	0.0016*
rTBF > 2.1	77.8	100	100	84.6	0.929	0.0012*

PPV positive predictive value, NPV negative predictive value, ADCMIN minimum absolute values of ADC, * Significance values (P > 0.05)

Multiplicity of tumor at midline has been considered to be the important characteristics of germinoma [20,21]. However, recent studies showed that midline multiplicity is not specific to germinoma, but is observed in NGGCTs as well [9,22]. Previous reports showed the utility of single voxel proton MR spectroscopy for the diagnosis of germinoma from other brain tumors via detecting high lipids peak [9,22]. However, both germinoma and NGGCT showed the characteristics high lipids peak, making it difficult to differentiate germinoma from NGGCT. Recent study showed that NGGCTs showed prominent hypointense foci in the parenchymal portion of the lesion on susceptibility-weighted imaging (SWI) or T2* gradient echo [23]. However, off midline germinoma also showed hypointense on SWI or T2*GRE. Moreover, differentiation from physiological calcification is difficult and require at least additional CT imaging. The utility of ADC obtained from DWI in the differential diagnosis of pineal region tumor is controversial [9,24,25]. The ADC value of germinoma is reported to be statistically lower than that of NGGCT [7]. ADC may be most useful for differentiation of immature teratoma component from germinoma [9]. However, physicians need to know that epidermoid like component of teratoma might be the cause of low apparent diffusion coefficient value. Wu et al. [8] reported combination of intratumoral T1 hyperintense foci and/or enhancing pattern with ADC was the best maker to differentiating CNS-GCT. Our results were consistent with their result, and we showed that high rTBF inside the tumor could give additional value for detecting NGGCT components. The advantage of ASL-PWI has been reported in other brain tumors [14,15], but there has been no report about the utility of ASL-PWI for CNS-GCT differentiation. Our results clearly showed that presence of high rTBF lesion would indicate "the GCT containing NGGCT part". Even in cases with the histological diagnosis of germinoma, the imaging characteristics of high rTBF part inside the tumor necessitates the physicians to diagnose the tumor as NGGCT.

Our studies have some limitations. First, the sample size is too

small for multivariate analysis. Second, we did not perform T1 FAT SAT imaging and we could not evaluate whether T1 hyperintense foci was originated from lipids/fat component or hemorrhage. Third, the method of ASL-PWI was not uniform as the MR machine was changed during this research period. Even with these drawbacks, our data supports the utility of ASL-PWI for detecting NGGCT components.

5. Conclusion

Our findings show that calculating rTBF by ASL-PWI is useful for detecting the NGGCT components. High relative blood flow lesion inside the histologically diagnosed germ cell tumor indicates the presence of NGGCT component, even in cases where the histology of the initial biopsied tissue might mislead the diagnosis by showing only germinoma component.

Declaration of competing interest

The authors declare that they have no known competing financial interests or personal relationships that could have appeared to influence the work reported in this paper.

Sources of funding

CRediT authorship contribution statement

Motoki Takano: Conceptualization, Data curation, Formal analysis, Software, Writing - original draft. **Yasuyuki Kinoshita:** Validation. **Kazuhiko Sugiyama:** Supervision, Validation. **Manish Kolakshyapati:** Writing - review & editing. **Takeshi Takayasu:** Writing - review & editing. **Ushio Yonezawa:** Data curation. **Akira Taguchi:** Data curation. **Yuji Akiyama:** Writing - original draft. **Vishwa Jeet Amatya:** Data curation. **Yukio Takeshima:** Validation. **Kaoru Kurisu:** Validation. **Fumiyuki Yamasaki:** Conceptualization, Formal analysis, Methodology, Writing - review & editing.

References

[1] Brain tumor registry of Japan (2001-2004), Neurol. Med. Chir. 54 (Supplement) (2014) 9–102.

[2] D.M. Ho, H.C. Liu, Primary intracranial germ cell tumor. Pathologic study of 51 patients, Cancer 70 (6) (1992) 1577–1584.

[3] K.W. Jung, J. Ha, S.H. Lee, Y.J. Won, H. Yoo, An updated nationwide epidemiology of primary brain tumors in republic of Korea, Brain Tumor Res. Treat. 1 (1) (2013) 16–23.

[4] Y.L. Suh, H. Koo, T.S. Kim, J.G. Chi, S.H. Park, S.K. Khang, G. Choe, M.C. Lee, E.K. Hong, Y.K. Sohn, Y.S. Chae, D.S. Kim, G.Y. Huh, S.S. Lee, Y.S. Lee, Tumors of the central nervous system in Korea: a multicenter study of 3221 cases, J. Neurooncol. 56 (3) (2002) 251–259.

[5] M. Matsutani, K. Sano, K. Takakura, T. Fujimaki, O. Nakamura, N. Funata, T. Seto, Primary intracranial germ cell tumors: a clinical analysis of 153 histologically verified cases, J. Neurosurg. 86 (3) (1997) 446–455.

[6] M. Matsutani, Combined chemotherapy and radiation therapy for CNS germ cell tumors–the Japanese experience, J. Neurooncol. 54 (3) (2001) 311–316.

[7] H. Ogiwara, Y. Tsutsumi, K. Matsuoka, C. Kiyotani, K. Terashima, N. Morota, Apparent diffusion coefficient of intracranial germ cell tumors, J. Neurooncol. 121 (3) (2015) 565–571.

[8] C.C. Wu, W.Y. Guo, F.C. Chang, C.B. Luo, H.J. Lee, Y.W. Chen, Y.Y. Lee, T.T. Wong, MRI features of pediatric intracranial germ cell tumor subtypes, J. Neurooncol. 134 (1) (2017) 221–230.

[9] F. Yamasaki, Y. Kinoshita, T. Takayasu, S. Usui, M. Kolakshyapati, M. Takano, S.Tsuyuguchi, V.J. Amatya, Y. Akiyama, Y. Takeshima, K. Sugiyama, K. Kurisu, Proton magnetic resonance spectroscopy detection of high lipid levels and low apparent diffusion coefficient is characteristic of Germinomas, World Neurosurg. 112 (2018) e84–e94.

[10] Y. Kinoshita, F. Yamasaki, A. Tominaga, T. Saito, T. Sakoguchi, T. Takayasu, S. Usui, K. Sugiyama, K. Arita, K. Kurisu, Pitfalls of neuroendoscopic biopsy of intraventricular germ cell tumors, World Neurosurg. 106 (2017) 430–434.

[11] R.P. Bokkers, M.J. van Osch, H.B. van der Worp, G.J. de Borst, W.P. Mali, J. Hendrikse, Symptomatic carotid artery

stenosis: impairment of cerebral autoregulation measured at the brain tissue level with arterial spin-labeling MR imaging, Radiology 256 (1) (2010) 201–208.

[12] B. Siewert, G. Schlaug, R.R. Edelman, S. Warach, Comparison of EPISTAR and T2*-weighted gadolinium-enhanced perfusion imaging in patients with acute cerebral ischemia, Neurology 48 (3) (1997) 673–679.

[13] D.J. Wang, J.R. Alger, J.X. Qiao, Q. Hao, S. Hou, R. Fiaz, M. Gunther, W.B. Pope, J.L. Saver, N. Salamon, D.S. Liebeskind, The value of arterial spin-labeled perfusion imaging in acute ischemic stroke: comparison with dynamic susceptibility contrast-enhanced MRI, Stroke 43 (4) (2012) 1018–1024.

[14] K. Yamashita, T. Yoshiura, A. Hiwatashi, O. Togao, K. Yoshimoto, S.O. Suzuki, K. Kikuchi, M. Mizoguchi, T. Iwaki, H. Honda, Arterial spin labeling of hemangioblastoma: differentiation from metastatic brain tumors based on quantitative blood flow measurement, Neuroradiology 54 (8) (2012) 809–813.

[15] H. Cebeci, O. Aydin, E. Ozturk-Isik, C. Gumus, F. Inecikli, A. Bekar, H. Kocaeli, B. Hakyemez, Assesment of perfusion in glial tumors with arterial spin labeling; comparison with dynamic susceptibility contrast method, Eur. J. Radiol. 83 (10) (2014) 1914–1919.

[16] G. Calaminus, R. Kortmann, J. Worch, J.C. Nicholson, C. Alapetite, M.L. Garre, C. Patte, U. Ricardi, F. Saran, D. Frappaz, SIOP CNS GCT 96: final report of outcome of a prospective, multinational nonrandomized trial for children and adults with intracranial germinoma, comparing craniospinal irradiation alone with chemotherapy followed by focal primary site irradiation for patients with localized disease, Neuro Oncol. 15 (6) (2013) 788–796.

[17] P. Wang, J. Li, Q. Diao, Y. Lin, J. Zhang, L. Li, G. Yang, X. Fang, X. Li, Y. Chen, L. Zheng, G. Lu, Assessment of glioma response to radiotherapy using 3D pulsed-continuous arterial spin labeling and 3D segmented volume, Eur. J. Radiol. 85 (11) (2016) 1987–1992.

[18] Y. Aihara, S. Watanabe, K. Amano, K. Komatsu, K. Chiba, K. Imanaka, T. Hori, T. Ohba, H. Dairoku, Y. Okada, O. Kubo, T. Kawamata, Placental alkaline phosphatase levels in cerebrospinal fluid can have a decisive role in the differential diagnosis of intracranial germ cell tumors, J. Neurosurg. 131 (3) (2018) 687–694.

[19] R. Awa, F. Campos, K. Arita, K. Sugiyama, A. Tominaga, K. Kurisu, F. Yamasaki, P. Karki, H. Tokimura, Y. Fukukura, Y. Fujii, R. Hanaya, T. Oyoshi, H. Hirano, Neuroimaging diagnosis of pineal region tumors-quest for pathognomonic finding of germinoma, Neuroradiology 56 (7) (2014) 525–534.

[20] V. Cuccia, D. Alderete, Suprasellar/pineal bifocal germ cell tumors, Childs Nerv. Syst. 26 (8) (2010) 1043–1049.

[21] D.C. Weksberg, Y. Shibamoto, A.C. Paulino, Bifocal intracranial germinoma: a retrospective analysis of treatment outcomes in 20 patients and review of the literature, Int. J. Radiat. Oncol. Biol. Phys. 82 (4) (2012) 1341–1351.

[22] A.A. Aizer, R.V. Sethi, E.T. Hedley-Whyte, D. Ebb, N.J. Tarbell, T.I. Yock, S.M. Macdonald, Bifocal intracranial tumors of nongerminomatous germ cell etiology: diagnostic and therapeutic implications, Neuro Oncol. 15 (7) (2013) 955–960.

[23] G. Morana, C.A. Alves, D. Tortora, J.L. Finlay, M. Severino, P. Nozza, M. Ravegnani, M. Pavanello, C. Milanaccio, M. Maghnie, A. Rossi, M.L. Garre, T2*-based MR imaging (gradient echo or susceptibility-weighted imaging) in midline and off-midline intracranial germ cell tumors: a pilot study, Neuroradiology 60 (1) (2018) 89–99.

[24] N. Dumrongpisutikul, J. Intrapiromkul, D.M. Yousem, Distinguishing between germinomas and pineal cell tumors on MR imaging, AJNR Am. J. Neuroradiol. 33 (3) (2012) 550–555.

[25] T. Kakigi, T. Okada, M. Kanagaki, A. Yamamoto, Y. Fushimi, R. Sakamoto, Y. Arakawa, Y. Mikami, T. Shimono, J.C. Takahashi, K. Togashi, Quantitative imaging values of CT, MR, and FDG-PET to differentiate pineal parenchymal tumors and germinomas: are they useful?, Neuroradiology 56 (4) (2014) 297–303.